

Electron impact double ionization of helium from classical trajectory calculations

Tihamér Geyer[†]

Department of Chemical Physics, Weizmann Institute of Science, Rehovot
76100, Israel

Abstract. With a recently proposed quasiclassical ansatz [Geyer and Rost, *J. Phys. B* **35** (2002) 1479] it is possible to perform classical trajectory ionization calculations on many electron targets. The autoionization of the target is prevented by a Møller type backward–forward propagation scheme and allows to consider all interactions between all particles without additional stabilization. The application of the quasiclassical ansatz for helium targets is explained and total and partially differential cross sections for electron impact double ionization are calculated. In the high energy regime the classical description fails to describe the dominant TS1 process, which leads to big deviations, whereas for low energies the total cross section is reproduced well. Differential cross sections calculated at 250 eV await their experimental confirmation.

PACS numbers: 34.10.+x, 34.80.Dp

Submitted to: *J. Phys. B: At. Mol. Opt. Phys.*

1. Introduction

Classical trajectory calculations of scattering processes have many advantages: they are easily implemented and robust and they provide an interpretation in terms of moving point particles, which is very familiar to our daily life’s experience [1]. But despite all their “beauty” and simplicity they have two serious drawbacks: they often are far from accurate and, what is even more limiting, they are conceptually restricted to one electron atoms — many electron atoms “autoionize”.

In a classical method, which starts from Bohr’s action quantization [2], only the hydrogen atom is stable. Actually this is the correct behavior: classical mechanics is the limit of very high quantum numbers. Consequently a classical hydrogen atom corresponds to a highly excited Rydberg state, which can only decay radiatively. It is therefore stable in the classical treatment. But a classical two electron atom resembles a doubly excited helium atom, which is only metastable — the “annoying” autoionization of a classical many electron atom is the correct physical behavior. To use such an unstable atom as a target in a classical trajectory calculation despite this difficulty two modifications of the Hamiltonian have been proposed: either the electron–electron interaction is neglected in the independent electron model (IEM)

[†] Present address: Zentrum für Bioinformatik, Universität des Saarlandes, D–66041 Saarbrücken, Germany

or, as in the “nCTMC” ansatz, additional stabilization potentials are included, which model the uncertainty relation [3] or place a bound on the accessible binding energies [4]. But these amendments are quantal additions onto the otherwise purely classical ansatz.

The stability problem might still be called a technical problem, but the fundamental difficulty remains: Bohr’s action quantization is a one dimensional rule only. It works for hydrogen, as this problem factorizes in spherical coordinates; each degree of freedom is quantized on its own. For the helium atom there exists no coordinate system in which all degrees of freedom separate. This is connected to the fact that some quantum numbers have to be replaced by “propensity rules” in a quantal description of the helium atom [5]. In the context of semiclassical calculations some multi dimensional quantization rules have been proposed, but they are limited to special geometries [6, 7]. Consequently there exists no prescription that would tell how to extend Bohr’s hydrogen model into a classical helium atom.

For the hydrogen target, where these two problems do not exist, the cross sections from a classical trajectory calculation are often not good — and therefore never were published — especially when angle differential cross sections are considered. The obvious way to try to improve the results is to modify the phase space description of the hydrogen target by including quantum mechanical information. This works to some extent, but leads either to unstable targets like the Wigner distribution [8, 9] or to the need for fit parameters [10]. Also with these alternate descriptions the initial values are not confined to the energy shell any more, an inconsistency that was neglected when extracting cross sections.

In a recent work we showed on electron impact ionization of atomic hydrogen how these fundamental problems can be overcome and the cross sections improved by a rederivation of the classical approximation of the time dependent quantum mechanical treatment [11]: the scattering process is first formulated quantum mechanically in the Møller picture and then all parts — the initial state, the scattering operator in its time dependent form and the final state — are simultaneously translated into Wigner’s formulation of quantum mechanics and only then approximated classically by setting $\hbar = 0$. The backward–forward structure of the resulting propagation scheme, a consequence of the Møller form of the scattering operator, refocuses the decaying classically approximated target onto the collision event. The energy spread of the initial state is dealt with by switching to cross sections differential in the energy transfer instead of using the absolute final energies of each trajectory. With this approach the cross sections on hydrogen could be improved greatly over a wide range of energies and geometries compared to the standard CTMC procedure. Even fully differential cross sections could be reproduced.

This quasiclassical approach now allows for arbitrary target descriptions, which do not need to be stable and need not be confined to the energy shell. There is also no fundamental limit on the dimensionality of the initial state, i.e., on the number of target electrons: the initial distribution to be used in the classical calculation is derived from the wave function and not from torus quantization according to quantum numbers, so the way to use multi electron targets in a CTMC like method is open. In a recent letter [12] we demonstrated that this dynamical stabilization through the propagation scheme in fact makes it possible to perform ionization calculations on classical helium targets. We calculated total single *and* double ionization cross sections on helium simultaneously without any modification of the interactions between all particles involved.

In this paper we will present further details of the calculation and show and interpret differential cross sections for electron impact double ionization of atomic helium.

2. The quasiclassical procedure

As mentioned above the quasiclassical approach is a classical approximation to quantum mechanical scattering, in which the quantum formulation is translated into phase space through the use of a correspondence rule [13, 14] and then approximated with $\hbar = 0$. This procedure was presented in detail in [11], so we just give a short summary and put the emphasis on these parts, which have to be adapted for multi electron targets.

2.1. Scattering operator and Møller propagation scheme

The backbone of the description is the scattering operator \hat{S} in the Møller formulation (see, e.g. [15]):

$$\hat{S} = \Omega_-^\dagger \Omega_+ \quad \text{with} \quad \Omega_\pm = \lim_{t \rightarrow \mp\infty} U^\dagger(t) U_0(t), \quad (1)$$

the Møller operators. The propagators $U(t) = \exp[-iHt]$ and $U_0(t) = \exp[-iH_0t]$ are defined in the usual way as the formal solution of the time dependent Schrödinger equation $\dot{\psi} = -iH\psi$ and describe the time evolution of ψ under the full and the asymptotic Hamiltonian, respectively.

This ansatz partitions the scattering process into three distinct stages, which are characterized by the considered interactions between the particles. The first and the last asymptotic propagation stages serve to construct the scattering states, which are solutions of the full Hamiltonian H , from the asymptotic initial and final states, which in turn are eigenfunctions of H_0^i and H_0^f , respectively. For electron impact ionization of atomic helium the full Hamiltonian has the following form:

$$H = \frac{p_p^2}{2} - \frac{Z}{r_p} + \frac{p_1^2}{2} - \frac{Z}{r_1} + \frac{p_2^2}{2} - \frac{Z}{r_2} + \frac{1}{|r_p - r_1|} + \frac{1}{|r_p - r_2|} + \frac{1}{|r_1 - r_2|} \quad (2)$$

H is given in atomic units, which we will use throughout the paper, if not otherwise denoted. The subscript p denotes the projectile, while the target electrons are labelled with 1 and 2. $Z = 2$ is the charge of the target nucleus, which we assume to have an infinite mass. In the asymptotic initial channel, described by

$$H_0^i = \frac{p_p^2}{2} + \frac{p_1^2}{2} - \frac{Z}{r_1} + \frac{p_2^2}{2} - \frac{Z}{r_2} + \frac{1}{|r_1 - r_2|}, \quad (3)$$

the projectile electron and the neutral helium target are independent, whereas in the asymptotic final state the ejected electrons do not interact with each other and the residual ion. We then have to distinguish between single and double ionization and we consequently have to consider two different asymptotic final Hamiltonians $H_0^{f(1)}$ and $H_0^{f(2)}$:

$$H_0^{f(1)} = \frac{p_a^2}{2} + \frac{p_b^2}{2} + \frac{p_c^2}{2} - \frac{Z}{r_c} \quad (4)$$

$$H_0^{f(2)} = \frac{p_a^2}{2} + \frac{p_b^2}{2} + \frac{p_c^2}{2} \quad (5)$$

The electrons are indistinguishable after the scattering event, we therefore label them with the subscripts a , b and c in the final state, where a has the highest and c the lowest final energy.

In the classical limit the Møller procedure translates into a propagation scheme, where each trajectory is first propagated backwards in time with H_0^i and then forward under H , i.e., with all interactions on. At first this may seem like superfluous effort, but this is the crucial difference to standard CTMC. It allows to use initial state distributions, which are not stationary under the approximated classical propagation: in the case of two electrons and a nucleus — the helium atom — one of the electrons will be ejected already in the initial backward propagation. When the propagation is reversed this ejected target electron is “brought back” into the atom. So when the projectile encounters the target both electrons have essentially returned their initial position. Because of this refocussing by the Møller propagation scheme there is no more need for any additional stabilization potentials, although all interactions are included correctly.

In a sense time has been reduced to a mere integration variable, as in the Møller formulation all the important events — the preparation of the initial state, the actual scattering process and the extraction of the cross sections — happen at the same “position” in time $t = 0$.

A different way to view the effect of the backward–forward propagation is the following: the classical approximation to the correct Wigner propagation neglects all terms containing \hbar , so errors are introduced. But, neglecting the approaching projectile for a moment, after going back and forth in time for the same interval the system returns to the same state again: the combined propagation in both directions gives the same final result as the correct Wigner propagation, only the intermediate steps, for which $t < 0$, are different. With the projectile added this is not completely true any more, but most of the error of the classical approximation is cancelled, when it comes to the target electrons.

2.2. The initial state distribution

In our quasiclassical approximation the initial distribution is constructed from the quantum mechanical wave function, which describes the initial state according to the asymptotic initial H_0^i . With our choice (3) this is a product wave of the free projectile electron and the helium target in its ground state. These two independent wave functions are translated into the Wigner picture [16] and then the product of their classical $\hbar = 0$ approximations is discretized, each discretization point serving as initial conditions for a trajectory in the above explained backward–forward propagation scheme.

Due to the $\hbar = 0$ approximation each of these trajectories evolves independently, but that does not imply that they are to be interpreted independently of each other. As the initial state is modelled by all initial values collectively, also their entirety only describes the scattering process. Remember that we still deal with a description in wave functions, though obscured by the classical approximation and the discretization.

For helium and more complex atoms there arises an additional difficulty compared to hydrogen: there the exact analytic wave function is known, whereas for helium only approximate wave functions of varying complexity have been formulated [17, 18, 19, 20, 21]. We therefore have to choose not only a prescription for how to translate the quantum wave function into a classical distribution [11, 13, 14, 16] but also an

appropriate wave function to start from.

For this first analysis we started from the most simple quantum mechanical ansatz for the helium wave function. We use the “ $1s^2$ ” product state of two identical hydrogenic ground state wave functions with an effective nuclear charge C . This product wave $\psi(r_1, r_2) = \text{H}1s_C(r_1) \text{H}1s_C(r_2)$ is then translated into a product of two identical classical phase space distributions.

$$\psi(r_1, r_2) = \frac{C^3}{\pi} \exp(-Cr_1) \exp(-Cr_2) \quad (6)$$

Independent of the nuclear charge this product wave function yields the minimum energy at $C = Z - 5/16$ [18], i.e., $C = 27/16$ for helium. This results in an energy of $E_t = -2.85$ a.u. (-77.5 eV), slightly less than the experimental value of -2.904 a.u. (-79 eV).

The angular electron–electron correlation is neglected in the initial wave function (6). Nevertheless we include the mutual repulsion of the target electrons in H_0^i , so their motion is coupled from the very moment the propagation is started. Of course, exchange correlation effects are beyond the reach of a classical approximation.

As shown by Cohen [14] a generalization of Weyl’s correspondence rule allows to derive nearly arbitrary recipes to set up the initial distribution within this quasiclassical ansatz. Each of them has different properties, which are important in different energy regimes, as was shown in [11]. We use three of the prescriptions described there, to convert the one electron wave functions $\text{H}1s_C$ of equation (6) into phase space distributions: (i) the “product” distribution [14], where the single electron wave function is translated into the product of the coordinate and momentum space densities, (ii) the “microcanonical” distribution [2], where each of the electrons is sampled according to a microcanonical distribution at an adapted one electron energy of -1.94 a.u., so that the (averaged) total energy, including the electron’s interaction, resembles that of the helium ground state and (iii) “Cohen’s energy distribution” [4], which is a superposition of microcanonical distributions with an energy dependent weight function, rescaled for the effective C .

To avoid clumsy wording we will label these distributions in the following as “product distribution”, “microcanonical distribution” and “Cohen’s (energy) distribution”, respectively, though these names are originally associated with the underlying one electron distributions.

In the calculations on hydrogen [11] the product distribution performed best for high energies, whereas Cohen’s energy distribution gave the best results at very low total energies. These two reproduce the density of the hydrogen ground state both in coordinate and momentum space. The microcanonical distribution, which is the only purely classically derivable distribution, has, due to its fixed binding energy, the wrong spatial density and gave worse results for all energies considered than any of the other distributions.

In addition to the density in phase space the energy spread $\sqrt{\Delta E_t^2} = \sqrt{\langle E_t^2 \rangle - \langle E_t \rangle^2}$ of the distributions turned out to be an important criterion, too. All three distributions have the same total energy of -2.85 a.u. = -77.5 eV, but their energy spread is quite different, see figure 1: the product distribution includes a rather wide range of energies with a spread of $\sqrt{\Delta E_t^2} = 5.71$ a.u. = 155 eV, which is twice the total energy of the target. Next comes Cohen’s energy distribution, which has $\sqrt{\Delta E_t^2} = 1.58$ a.u. = 43 eV. The spread of the microcanonical distribution is determined only by the variation in the distance between the two electrons; it has

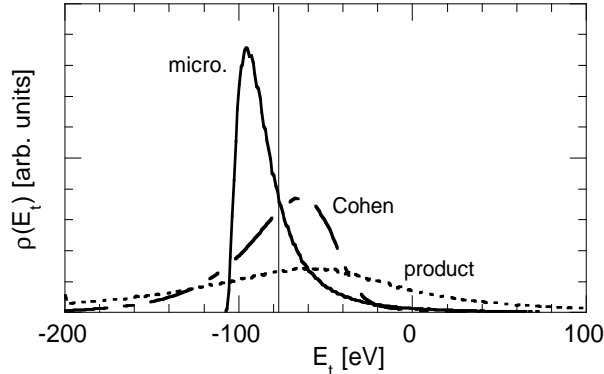


Figure 1. Distribution of the target energy when the initial conditions are chosen according the “microcanonical” distribution (—), “Cohen’s energy distribution” (---) and the “product” distribution (- - -). The thin vertical line marks the average binding energy of -2.85 a.u.

consequently the smallest value of only 1.18 a.u. = 32 eV.

In the next section we will confirm that the actual value of the total energy of the initial distribution is of secondary interest only, because the correct ionization potential is used to extract the cross sections, not the (wrong) binding energy of the initial state.

2.3. The cross section

In the quantum mechanical formulation the fully differential cross section is calculated from the squared overlap between the scattered wave function $|\psi_s\rangle = \hat{S}|\psi_i\rangle$ and the given final state $|\phi_f\rangle$. This overlap scalar product then translates into a phase space integral of the scattered distribution ρ_s times the classical approximation of the projector onto the final state \mathcal{P}_f .

$$|\langle\phi_f|\psi_s\rangle|^2 \Rightarrow \int dr dp \mathcal{P}_f \rho_s \quad (7)$$

According to the final state Hamiltonians for single and double ionization, equations (4) and (5), the free electron wave functions are plane waves. The corresponding projector consequently is a product of momentum delta functions, which are then reformulated in final angles and energies.

We include the symmetrization of the electrons into the final state, which means that in the classical approximation we have to consider all permutations of the electrons in \mathcal{P}_f when calculating the overlap scalar product.

We see that the cross section is determined at first by the (discretized) scalar product between wave functions, translated into phase space, and only secondly by the acceptance region of a macroscopic classical detector. This is not a technical difference to the classically derived standard CTMC, but one of interpretation: in this quasiclassical context one should refrain from “interpreting” single trajectories as the paths of real electrons, they are only time dependent discretization points in phase space.

From equation (7) we easily see how to deal with excitation cross sections in this quasiclassical approach: the final state projector \mathcal{P}_f then explicitly includes the final

bound state of the excited target electron according to the translation rule chosen for the initial state (cf. section 2.2). To calculate the excitation cross section the final values of all trajectories are summed up with a weight according to the final excited state's phase space density. Special care has to be taken to ensure that the phase space densities chosen to represent the bound orbitals are orthogonal in order to conserve probability.

An ansatz to use final state densities modelled after the quantum wave functions along the lines of Eichenauer *et al* [8] and Hardie and Olson [10] was recently introduced by Sattin [22]. There microcanonical distributions are added up according to a weight function depending on the orbits' energy.

The classically derived prescriptions for binning the trajectories' final values, on the contrary, are based on action angle quantization [23, 24].

The final state now has a fixed total energy, but our initial state, and consequently the scattered distribution ρ_s , too, is not confined to the energy shell. The overlap with the on-shell final state would consequently cut out of the whole ρ_s only those trajectories, which initially had started on the energy shell, i.e., only a part of the initial distribution would actually be used. This is both a conceptually unsatisfying situation and a problem of normalization.

To solve this issue we switch to cross sections differential in energy transfer, as explained for the hydrogen target in reference [11]. The energy difference ΔE_p for the projectile electron is defined as the difference between the final and the initial energy,

$$\Delta E_p = E_p^f - E_p^i, \quad (8)$$

with $E_p^f = \frac{p_f^2}{2}$ and $E_p^i = \frac{p_i^2}{2}$. For the electrons of the helium target the electron-electron repulsion in the initial state has to be accounted for, too, as it is released in the ionization process. For the initially bound electrons the energy transfer is consequently defined as, here written without the subscripts 1 or 2:

$$\Delta E = E^f - E^i = \frac{p_f^2}{2} - \left(\frac{p_i^2}{2} - \frac{Z}{r_i} + \frac{1}{2} \frac{1}{r_{12}} \right) \quad (9)$$

All final states, which contribute to double ionization, are characterized by three free electrons, i.e.,

$$-\Delta E_p > IP_1 + IP_2 \quad \text{and} \quad \Delta E_1, \Delta E_2 > \frac{IP_1 + IP_2}{2}. \quad (10)$$

$IP_1 = 24.6$ eV and $IP_2 = 54.4$ eV are the (positive) ionization potentials for the first and the second electron, respectively: the projectile has to supply enough energy to ionize both electrons.

For single ionization two of the three electrons are free and the third is still bound, i.e., we get the following conditions for the energy transfers, which have to be tested with electrons 1 and 2 exchanged, too:

$$-\Delta E_p > IP_1, \quad \Delta E_1 > \frac{IP_1 + IP_2}{2} \quad \text{and} \quad \Delta E_2 < \frac{IP_1 + IP_2}{2} \quad (11)$$

These requirements may seem asymmetric at first sight, but when one electron is ionized, the interaction energy between the target electrons, which is the difference between IP_1 and IP_2 , is released, too, making up for the difference between ΔE_p and $\Delta E_1 + \Delta E_2$ (see equation (9)).

Apart from this selection through the final state another constraint has to be considered, which originates in the Møller propagation scheme: the central forward

propagation can only be reversed into the final backward leg, if those interactions, which have to be switched off from H to $H_0^{f(1)}$ or $H_0^{f(2)}$, respectively, have vanished sufficiently. To turn off the nucleus–electron interaction an electron has to be far away from the nucleus, but it can only get away if it is not bound, i.e., if its actual energy is positive:

$$E^f = \frac{p_f^2}{2} - \frac{Z}{r_f} > 0. \quad (12)$$

For the total cross section for single or double ionization therefore the summation over contributing final states (7) satisfying the constraint from the Møller scheme (12) amounts to counting those trajectories, for which both the energy transfers, equations (11) and (10), are correct and the actual energies (12) of two or three electrons are positive, respectively. With these sums, $N^{(1)}$ and $N^{(2)}$, the absolute cross sections are calculated in the usual CTMC way from the maximum impact parameter B_0 and the total number N of propagated trajectories:

$$\sigma^{(1)} = \frac{\pi B_0^2}{N} N^{(1)} \quad \text{and} \quad \sigma^{(2)} = \frac{\pi B_0^2}{N} N^{(2)} \quad (13)$$

The single ionization cross section also includes events, in which the remaining electron is excited.

The recipe for how to extract cross sections is transferred into the classical form independently of the initial state description. This is the reason why we do not refer to the smeared binding energy E_t of the initial distribution, but to the experimentally observed correct ionization potentials IP_1 and IP_2 . Any initial state can be used, independent of its energy; one might even fancy two electrons without a nucleus localized in space according to the quantum densities — a setup with a positive total energy. But an electron would be considered ionized only when enough *additional* energy has been transferred onto it.

3. Results

Up to now we have repeated and detailed how the quasiclassical procedure has to be set up to calculate electron impact ionization on atomic helium. That the propagation scheme actually refocuses the autoionizing helium target has been shown in a recent letter [12]. We now present and discuss the total cross sections for single and double ionization and then confirm our findings through differential cross sections.

3.1. Total cross sections

With the three initial distributions explained above the total ionization cross sections $\sigma^{(1)}$ for single ionization and $\sigma^{(2)}$ for double ionization are calculated. The results are compared to measurements by Shah *et al* [25] in figure 2. The differences between the initial distributions are only small both for $\sigma^{(1)}$ and $\sigma^{(2)}$: all three distributions lead to the same shape of the cross sections while the absolute value differs in a range of about $\pm 15\%$. Therefore figure 2 only shows the results from the product distribution. The result from the microcanonical distribution is slightly higher, while Cohen’s energy distribution leads to a slightly smaller total cross section. A similar behavior had occurred already for the total cross sections on hydrogen, calculated in [11].

The single ionization cross section $\sigma^{(1)}$ agrees with the measurement on the level expected from a classical trajectory calculation: the overall coincidence is reasonable,

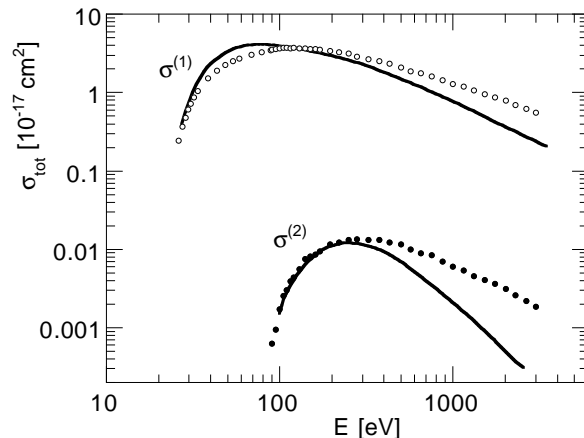


Figure 2. Total cross sections $\sigma^{(1)}$ for single and $\sigma^{(2)}$ for double ionization: Comparison of our results (solid lines), calculated with the “product” distribution (see text), with the experimental data of Shah *et al* [25] (open and filled circles).

but the absolute value at the maximum is slightly too high, the maximum itself is shifted to lower energies by a factor of about two and the high energy behavior follows the classical $1/E$ decay [26] instead of the correct Bethe–Born limit of $\ln(E)/E$ [27].

This cross section had been calculated previously by Schultz *et al*, both in the independent electron model and with the nCTMC procedure [28]. Our calculation with the microcanonical distribution reproduces the nCTMC result, which is closer to the experiment than the IEM model. This is not surprising, as the nCTMC initial state can be viewed as a symmetric subset of our microcanonical description. The additional stabilization potential used there prevents autoionization before the scattering event and then essentially vanishes, once one of the target electrons is ionized.

Before we actually look at our results for the double ionization cross section $\sigma^{(2)}$, we want to contemplate, which high energy behavior can be expected from a classical description: again, as with $\sigma^{(1)}$, quantum effects like tunneling are not accounted for in the classical treatment. Additionally the so called shake-off process, which is dominant for double ionization at very high energies [29], can not be modelled classically: When in the classical description one of the electrons is removed then there is no quantization condition as in quantum mechanics, which “forces” this electron to change its orbit to one of the allowed ones — either to one of the discrete bound levels or to the continuum. Classically any orbit at any binding energy is allowed, so there is no need for a transition; and consequently no shake-off process. In the classical treatment even an opposite effect occurs: when one of the target electrons is removed, the remaining ion is actually “stabilized” in its current (excited) state, because with the other target electron the cause for autoionization is removed.

Though the shake-off process does not exist in the classical description, there are still two important processes left, which lead to double ionization: in the so called “Two-Step 1” (TS1) process the projectile ionizes one of the target electrons, which in turn ionizes the other one in a subsequent ($e, 2e$) reaction. The probability for the second ionization only depends on the energy spectrum of the first electron and is therefore nearly independent of the projectile energy. In the classical description

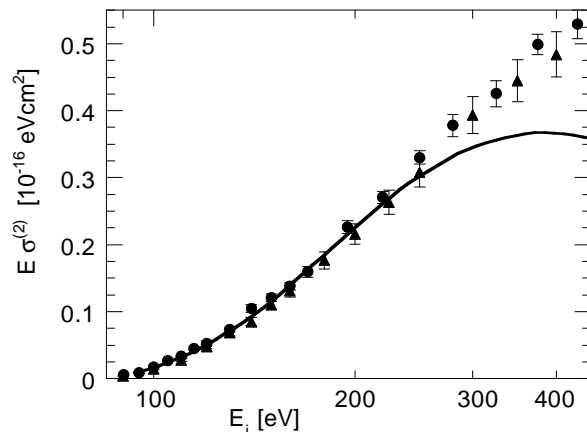


Figure 3. Bethe like plot of the double ionization cross section $\sigma^{(2)}$: comparison of our quasiclassical calculation with the product distribution (solid line) to the experimental results of Shah *et al* [25] (circles) and of Rejoub *et al* [31] (triangles). For better comparison with figure 2 the impact energy is not scaled with the ionization threshold.

the TS1 process consequently should decrease roughly proportional to the single ionization’s $1/E$ law. The other process, the “Two-Step 2” (TS2) process, consists of two independent encounters between the projectile and the two target electrons. Each collision’s probability falls off as $1/E$, so the TS2 decays proportional to $1/E^2$. Therefore it can be deduced from the high energy behavior of $\sigma^{(2)}$, if the TS1 or the TS2 process is dominant in the classical description.

Looking at the results for the double ionization cross section $\sigma^{(2)}$ in figure 2 we see that for high energies it decreases much faster than $\sigma^{(1)}$ — in fact it follows a $1/E^2$ behavior for $E > 600$ eV — while the experimental results confirm the constant asymptotic ratio of $\sigma^{(2)}/\sigma^{(1)}$ derived from quantal calculations [29].

We therefore may conclude, that in classical trajectory calculations the double ionization at very high energies mainly happens through the “Two-Step 2” (TS2) mechanism, whereas the TS1 seems to be missing. To verify this hypothesis, which contradicts the experimental evidence [30], we have to look at differential cross sections.

For energies below the maximum of the cross section, on the other hand, the experimental results of $\sigma^{(2)}$ are much better reproduced than for $\sigma^{(1)}$.

The correspondence between the quasiclassical results and the experimental data at low energies can be seen more pronounced, if a Bethe plot like presentation is chosen: figure 3 plots the product of the total energy and $\sigma^{(2)}$ against the impact energy, our results with the product distribution as well as experimental data from Shah *et al* [25] and Rejoub *et al* [31]. The cross section is in nearly perfect agreement with the measurements from low impact energies up to about 250 eV. For impact energies above 250 eV our calculation falls back against the experimental results. Against common experience and the usual interpretation of the correspondence principle high energies in electron impact ionization obviously do not mean that the system becomes more “classical” — on the contrary, the description becomes worse and worse, the higher the energies become. Further classical calculations should therefore focus on

the low energy regime, where the correlated dynamics of all four particles becomes more and more complex and even chaotic. Therefore it is not possible to make a simple prediction about the ionization mechanism at intermediate and low energies. It is only right above the threshold where a highly symmetric final state configuration and a power law behavior is predicted by a Wannier type argument [32, 33].

With these arguments it is understandable that in the classical calculation $\sigma^{(2)}$ is reproduced much better at low energies than $\sigma^{(1)}$: due to the higher dimensionality of the phase space there exist more classical reaction paths for double than for single ionization, which renders quantum effects less important than when only one electron is removed.

If we attribute the difference between our results and the experiment to the missing TS1 process, as explained above, then we can estimate that the probability for the sequential TS1 is negligible below about 250 eV. For a TS1 event to be possible at 250 eV the projectile has to transfer about one third of its energy onto one of the target electrons, which is already a rather “violent” collision. For higher impact energies the TS1 process then becomes increasingly important and we can estimate from the difference between our calculated $\sigma^{(2)}$ and the experiment that at $E_i \approx 500$ eV both processes contribute with equal weight to double ionization. With fully differential cross sections a “great importance of second- or higher-order effects” at 600 eV has been observed by Lahmam–Bennani *et al* [34].

For double ionization there is, for obvious reasons, no CTMC comparison available yet. Our result is the first classical trajectory calculation for double ionization with two active target electrons without additional stabilization potentials or the need to “switch off” the interaction between the target electrons.

It should be emphasized, that the absolute cross sections for both single and double ionization can be calculated from the same run of the program. For both cases the same initial distribution is used and both target electrons are explicitly included. In principle excitation could be included in the analysis, too, though here we confine ourselves to ionization alone. This is parallel to the experiment, where single and double ionization and excitation all occur concurrently.

It was not clear a priori, though, if this would really work. For single ionization, e.g., the second electron, which is not ionized, might not act as an independent spectator and could disturb the single ionization process.

In an IEM treatment it is for methodological reasons not possible to calculate all processes simultaneously: there the electron–electron repulsion in the target is neglected and therefore only one of the two thresholds for single *or* for double ionization can be described correctly. The same difficulty arises in the nCTMC treatment due to the restricted symmetric geometry of the initial distribution.

In an actual calculation it is more efficient, though, to run the calculation twice with two different maximal impact parameters: a bigger one for $\sigma^{(1)}$ to cover the whole target area and a smaller one to achieve enough statistics for the much rarer double ionization, where both target electrons have to be located around the path of the projectile. Typical maximal impact parameters are $B_0 \approx 30$ a.u. for single and $B_0 \leq 3$ a.u. for double ionization. Then at each impact energy about 10^5 trajectories are necessary for sufficiently small statistical errors of the total cross section.

The propagation of the electrons’ trajectories is performed by a symplectic integrator, which separates the attractive regularized electron–nucleus interaction from the electrons’ mutual repulsion (for details please see reference [11]). This algorithm is extremely stable, as it even allows the electrons to fall “into” the nucleus.

	N_t	N_2	B_0
Cohen	310 Mio.	33447	1.2 a.u.
product	39 Mio.	7617	1.5 a.u.
microcan.	50.6 Mio.	19740	1.2 a.u.

Table 1. Number of trajectories N_t and double ionization events N_2 for the three initial state distributions at $E = 2$ keV together with the maximal impact parameter B_0 (see text).

To calculate differential cross sections huge numbers of trajectories have to be run and the number of faulty trajectories has to be much smaller than the few trajectories that contribute to a given cross section. Typical fractions of trajectories which had to be discarded are on the order of one per every ten million trajectories, which is smaller than the yield of double ionization events by at least three orders of magnitude.

3.2. Differential cross sections at high energies: $E_i = 2$ keV

The total double ionization cross section at high energies falls off as $1/E^2$, which is much faster than the experimental data. This had lead us to conclude that in this regime double ionization essentially occurs through independent collisions between the projectile and each of the two target electrons. But now we need to verify this conjecture, because the difference between our calculation and the experiment might also be caused by the classical approximation itself, i.e., that the occurring processes are modelled correctly, but only the overall probability is too small due to the description of the electrons as classical point particles.

We therefore ran calculations at an impact energy of 2 keV, which is well into the high energy regime. At this energy single and double differential cross sections were measured by Dorn *et al* [35]. The numbers of trajectories calculated with the three initial state descriptions and the resulting double ionization events are given in table 1. To increase the number of double ionization events the impact parameter of the projectile was sampled linearly between 0 and B_0 ; in the analysis each trajectory then is weighted with an additional factor of $\frac{b}{2B_0}$. Therefore the total double ionization cross section can not be calculated from the values given in table 1 alone but only from the saved trajectory data.

The two “classical” ionization processes, the TS1 and the TS2, lead to different signatures in the angular and energetic distribution of the ejected electrons. They are already discernible in partially differential cross sections: at this high impact energy the energy loss of the projectile is much smaller than its initial energy, the final channel therefore consists of one fast and two slow electrons. These two slow electrons repel each other on their way out; ejection into the same half sphere is consequently suppressed. Due to the two independent collisions this is the main angular signature of the TS2 process. In the TS1 process, on the other hand, the momenta of the two slow electrons are correlated because of the second ($e, 2e$) process. This elastic collision between two particles of identical mass leads to a peak in the relative angle between the slow electrons in the range between about 90 and 110 degrees, depending on the relative energy partitioning and the momentum transferred.

This angle between the two slow electrons is plotted in figure 4 for an impact energy of 2 keV: our results are compared to polynomial fits of the measurements of Dorn *et al* [35]. The relative angle is integrated over all pairs of slow electrons, which

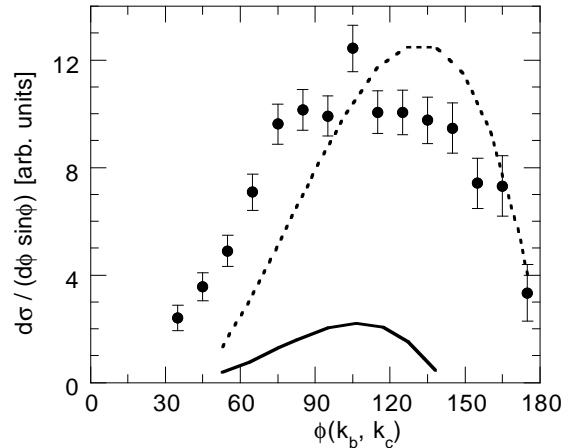


Figure 4. Angle Φ between the two slow ejected electrons at double ionization with $E_{in} = 2$ keV integrated over all energies $E_b + E_c < 35$ eV: comparison of our results (full circles) with polynomial fits of the experimental results of Dorn *et al* [35] ($E_b + E_c < 20$ eV) for small recoil ion momentum (solid line) and for small momentum transfer (broken line).

have a sum energy of $E_b + E_c < 35$ eV in the calculation and $E_b + E_c < 20$ eV in the experiment. The experimental data are given for two different kinematical regimes, discerned by the momentum transfer of the projectile q and the recoil ion's momentum. Both the experimental curves show a distinct peak, whose position varies with the momentum transfer. Our results, on the other hand, show a broad distribution of angles, whose only feature is the suppression of small relative angles due to the electrons' mutual repulsion. The form of the angular distribution is independent of both the momentum transfer and the maximum sum energy, only the number of contributing events varies. The angular distribution is essentially independent of the relative energy partitioning $\epsilon = \frac{E_b}{E_b + E_c}$, too.

This behavior is consistent with the hypothesis that at high energies in the classical descriptions the TS2 process is dominant, contrary to the experimental evidence.

The two considered processes, the TS1 and the TS2, can be discerned, too, by comparing the joint distribution of the slow electrons' final energies: at these high impact energies the energy transfer is much smaller than E_i , so that on the average in the two collisions of the TS2 twice as much energy is transferred onto the target electrons than in the one collision of the TS1. In the TS1 this energy is then shared between the two target electrons. The energy distribution of electrons ionized in a TS2 process should therefore be about twice as wide as the one of electrons from the TS1 process.

The distribution of energies of the two slow electrons is plotted in figure 5. Panel (a) shows the experimental data of Dorn *et al* [36], whereas our quasiclassical result with Cohen's initial distribution is shown in (b). At first glance both results seem to be similar, but it is important to note that in (b) the scale of the energy axes is twice as wide as in (a).

The dip in the experimental cross section where both energies are small is due to the time resolution of the spectrometer: events, in which the longitudinal momentum

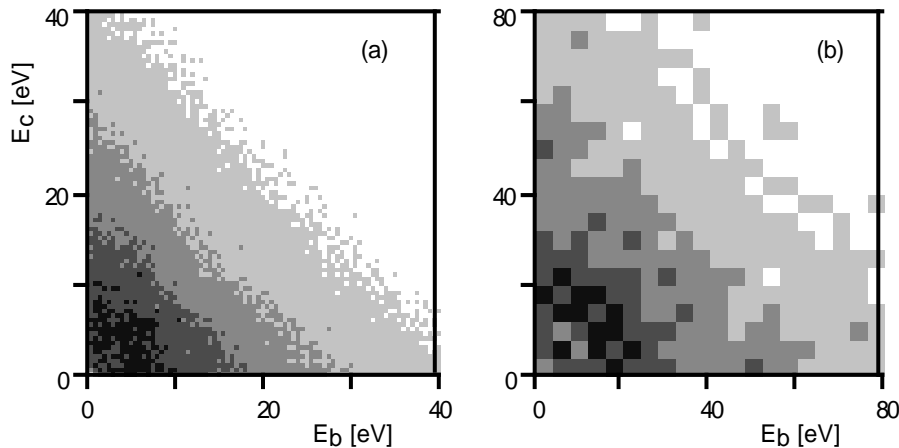


Figure 5. Joint distribution of the energies E_b and E_c of the two slow electrons for $E_{in} = 2$ keV: comparison of the experimental result of Dorn *et al* [36] to our calculation with Cohen’s distribution. Note that the energy scales of the two plots differ by a factor of two.

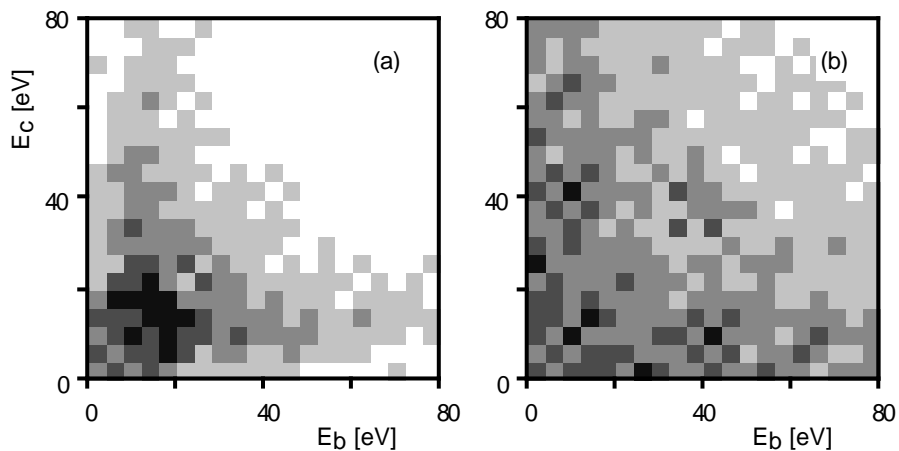


Figure 6. Same as figure 5: results from the calculations with (a) the microcanonical initial distribution and (b) with the product target description.

difference between the slow electrons is less than $|p_b - p_c| < 0.3$ a.u. could not be resolved in this experiment. When both energies are small, then the relative momentum is also small. This restriction is included in our result, too.

Figure 6 shows the same cross section calculated with the microcanonical distribution (a) and with the product initial state description (b). The effect of the different initial state descriptions can clearly be seen: with the microcanonical distribution the very asymmetric events are missing, i.e., when one of the ejected electrons only has a small energy. The explanation is connected to the form of the energy spread of the initial distribution, see figure 1: both electrons are sampled independently at the same fixed one-electron energy. Consequently the spread of the total energy is determined solely by their interaction — but as their distance is limited

there is a lower limit for this contribution, and therefore for the total energy of the target initial conditions. There is no upper limit for the electron–electron repulsion, therefore, to achieve the correct average binding energy, most of the initial values must have a binding energy of less than the average to compensate for the relatively few events, where the interaction energy is high. These initial conditions with energies below the average are harder to ionize within our scheme, which requires the electrons to be actually free in the end. As the final energies increase this threshold blocks less and less events that have the correct energy transfer and then the cross sections resemble that from Cohen’s distribution (figure 5(b)).

This again shows that an initial distribution which is constructed from a classical recipe may have unphysical properties — here the hard limits in the radial and the energy distributions — and lead to problems, when used in a quantum mechanically derived context.

With the product distribution, figure 6, the energies of the two slow electrons are spread out to even higher values compared to Cohen’s distribution. This is the consequence of the very broad energy spread of the initial state, which is about twice as wide as the distribution of final energies resulting from the ionization process. But it is not our method which breaks down. The energy of each trajectory is still well defined. This very wide initial energy spread means that there are many “extreme” initial values, i.e., trajectories, in which the electrons are started with high momenta at large distances from the nucleus, with low momenta at small distances or with a very small interelectronic distance. Trajectories started there are far more likely to end “outside” the main features of the cross section and therefore blur the result.

Summarizing, one can say that the evidence presented — the high energy behavior of $\sigma^{(2)}$, the distribution of the inter–electron angle and the energies of the slow electrons — confirms that at high energies a (quasi) classical treatment of double ionization can not describe the important processes. In general the coupling between the target electrons is grossly underrepresented. The reason for this behavior originates in the description of the electrons as point particles: when the first electron is not kicked exactly into the direction of the other target electron, the second stage of the TS1 process can not take place. Obviously, in most cases the first electron is ejected so that the other electron does not “notice” it. Or in other words: for the first electron to ionize the other, it has to be kicked into a very narrow cone around the vector connecting the two electrons’ positions. In the quantum mechanical treatment both electrons are located spherically symmetric around the nucleus; the first ionized electron always has to pass “through” the other electron. Therefore the subsequent ionization can take place independent of the direction in which the first electron leaves the atom.

This shortcoming of the classical approximation is independent of the initial state’s description, though the results show that it is nevertheless important to choose the best possible distribution: an inappropriate initial distribution can only make the results worse.

It is interesting to note that recently photo double ionization has been described amazingly well in a mixed quantum classical picture [37]. In the classical part, which models the sequential “TS1” process the electron that absorbs the photon starts “on” the nucleus. From this highly symmetric starting point it always has to pass through the probability distribution of the other electron and the chance for their encounter is independent of the initial direction of the first electron.

	N_t	N_2	B_0
Cohen	64.3 Mio.	83581	1.5 a.u.
product	130 Mio.	35785	3 a.u.
microcan.	34.8 Mio.	49277	3 a.u.

Table 2. Number of trajectories N_t and double ionization events N_2 at $E_{in} = 250$ eV for the three initial state distributions together with the maximal impact parameter B_0 (see text).

3.3. Differential cross sections at $E_i = 250$ eV

For low impact energies up to about 250–300 eV the agreement between the measured and the calculated total double ionization cross section is remarkably good, see figure 3, suggesting that in this energy regime the quasi classical treatment should be able to describe those dynamics, which are actually taking place. Unfortunately there are no measurements of electron impact ionization of helium available yet in this energy regime, though first results of kinematically complete experiments at 500 eV are just being reported [38] and results from even lower impact energies will surely follow. We decided not to perform calculations at $E_{in} = 500$ eV at this point, because of what we learned above from the results at $E_{in} = 2$ keV we expect them to be at most partly correct. So we can not compare our results to an experiment yet, but it will nevertheless be instructive to look at the available quasiclassical results and predictions.

The numbers of trajectories calculated and the resulting double ionization events for the three initial distributions are summarized in table 2. The impact parameter was sampled linearly again as for 2 keV.

The different spatial form of the microcanonical distribution, which was explained in section 2.2, is reflected in these numbers, too: to achieve a comparable number of double ionization events N_2 with the product distribution about four times as many trajectories had to be run. The resulting total $\sigma^{(2)}$ is nearly the same, though. This means that with the microcanonical distribution double ionization on average takes place at an impact parameter, which is about four times larger — the target electrons are found at larger radii.

Now, at $E_{in} = 250$ eV, the projectile electron is only about twice as fast as the classical target electrons; the dynamics is much slower than at 2 keV and it can be expected that the distinction between the fast projectile and the slow ionized target electrons vanishes.

This effect can already be seen when the angle differential cross sections $\frac{d\sigma}{d\theta}$ of the fastest final electron and of the former projectile after a double ionization event are compared, see figure 7. At $E_{in} = 2$ keV the two cross sections are indiscernible (not shown here), but now they differ by about 10 % in the forward direction and even more for angles larger than 60° . The projectile is still emitted preferentially into the forward direction, but in one of about every ten double ionization events it transfers so much of its energy onto the target electrons that one of these becomes the fastest. These fast ionized target electrons then show up in figure 7 in the direction perpendicular to the incident projectile, i.e., at angles between 60° and 120° . When the projectile is scattered backwards, i.e., $\theta > 135^\circ$, it had to reverse its momentum. This big energy transfer makes that in the backward direction the projectile is rarely the fastest electron.

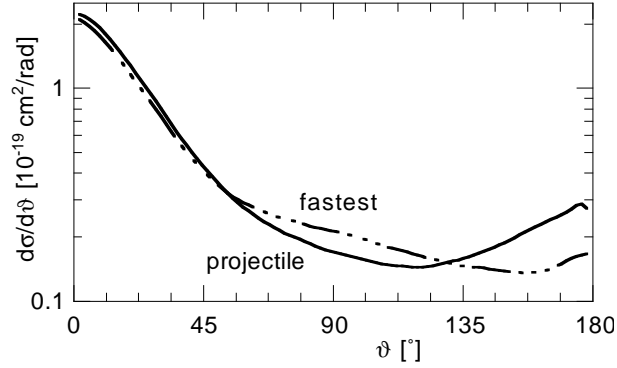


Figure 7. Angle differential cross $\frac{d\sigma}{d\theta}$ at $E_{in} = 250$ eV for the fastest final electron (broken line) and the former projectile electron (solid line) after a double ionization event.

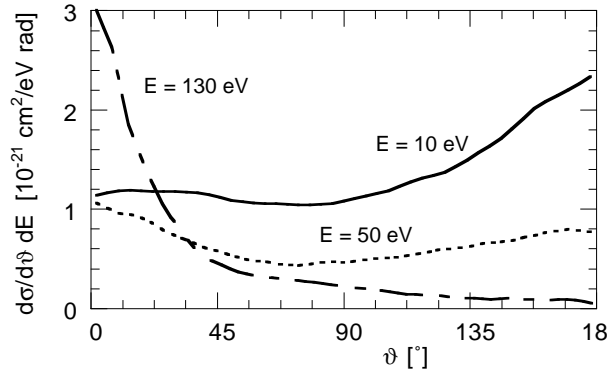


Figure 8. Doubly differential cross section $\frac{d\sigma}{d\theta dE}$ for double ionization at $E_{in} = 250$ eV for the fixed final electron energies of 10 eV (—), 50 eV (- -) and 130 eV (- · -). The calculation was performed with Cohen's distribution.

In an experiment the distinction between the former projectile and the target electrons is not possible. The angular distribution of the electrons is usually measured for a fixed final energy. Of course, this type of cross section can be extracted from our calculations, too, see figure 8: it plots the absolute doubly differential cross section $\frac{d\sigma}{d\theta dE}$ for double ionization, integrated over all three electrons, for the fixed final energies of 10 eV, 50 eV and 130 eV, calculated with Cohen's initial distribution. Again, as already in figure 7, the fast electrons (130 eV) are emitted preferentially into the forward direction, while the slowest electrons (10 eV) are ejected into the rear half sphere. The crossover between the emission in forward and in backward direction takes place at an electron energy of 50 to 60 eV, which is about a third of the total energy of the system.

An overview over the behavior of $\frac{d\sigma}{d\theta dE}$ is given in figure 9: it plots this cross section as a function of both the angle θ and the final one electron energy E . The dominant structures of this cross section are the maximum for fast electrons with an energy around 130 eV and small angles up to about 20° and the broad angular distribution of the slow electrons with an emphasis on the backward direction. As

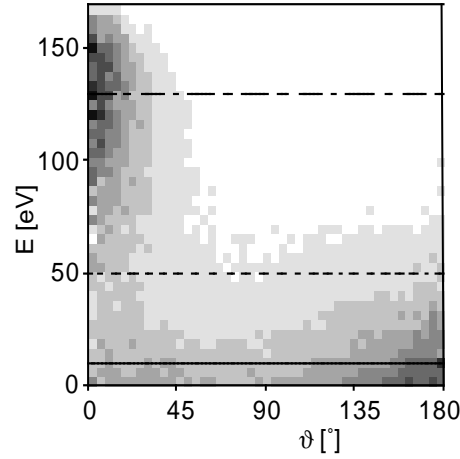


Figure 9. Doubly differential cross section $\frac{d\sigma}{d\theta dE}$ at $E_{in} = 250$ eV, integrated over all electrons. The greyscale is linear between 0 and the maximum value in arbitrary units. The three horizontal lines correspond to the cross sections at the fixed energies plotted in figure 8.

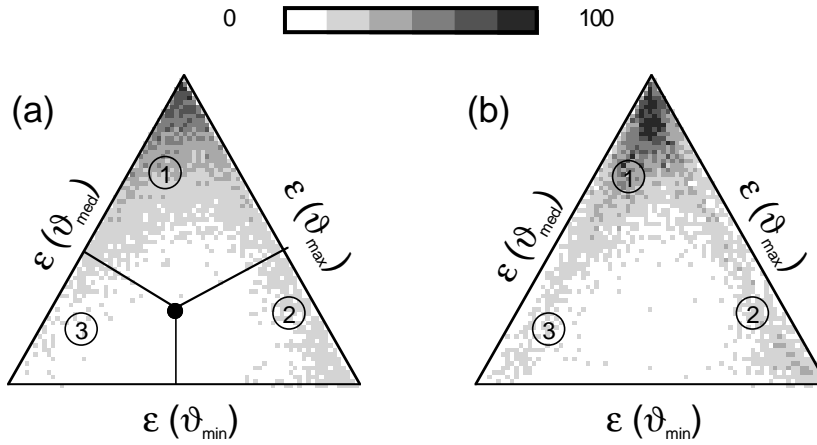


Figure 10. Dalitz plot of the three electrons' final energies, calculated with Cohen's distribution (a) and with the microcanonical initial distribution (b). The greyscale is linear between 0 and the maximal value for each plot. The different energy partitions, which correspond to the numbers inside the triangles, are explained in the text.

said before, the crossover between the two angular patterns takes place around 50 eV.

Both figure 8 and 9 are not very sensitive to which initial distribution has been used; the differences are the same as those already observed at the slow electrons' joint energy distributions, see figures 5(b) and 6: with the microcanonical distribution the events with very small final energies are missing again and with the product distribution both the distribution of the angles and the energies is broadened.

The cross sections at $E_{in} = 250$ eV shown until now were extracted from the double ionization events, but they did not test for any correlation between the outgoing

electrons.

At 2 keV the projectile is much faster than the ionized target electrons; the correlation between the electrons affects mainly the “subsystem” of the two slow electrons. The presence of the fast projectile can conveniently be reduced to a momentum and energy transfer onto the otherwise independent target system. But now, at $E_{in} = 250$ eV, where the dynamics is much slower and the three final energies are closer together this separation is at best questionable. We therefore need a way to plot the final energies and angles, which is sensitive to correlations between the three particles.

One possibility is the so called Dalitz plot [39]: it places the relative final energies $\epsilon_i = \frac{E_i}{E_a + E_b + E_c}$, with $i = a, b, c$, of the three electrons inside an equilateral triangle, cf. figure 10. As $\epsilon_a + \epsilon_b + \epsilon_c = 1$ each combination of final energies is mapped unambiguously onto one point inside the triangle, for which the distances from the three sides have the same ratios with each other as the relative energies. This representation of the energies of three correlated particles was first used in high energy physics, but has recently been adapted in atomic physics, too, e.g., for the fragmentation of H_3^+ [40] or for triple ionization by fast heavy ion impact [41]. We follow this work of Schulz *et al* and sort the final relative energies ϵ_i according to the corresponding scattering angle θ_i : the relative energy of the electron with the smallest $\theta = \theta_{min}$ is measured from the base of the triangle, the ϵ for the biggest $\theta = \theta_{max}$ from the right side and the intermediate $\epsilon(\theta_{med})$ from the left side.

Figure 10 shows the resulting distributions, when Cohen’s distribution is used as the target initial state in panel (a) and with the microcanonical distribution in (b). Their overall structure is similar: the maximum is at the top of the triangles, which means that the highest (relative) energy mainly goes with the smallest scattering angle. This is consistent with the cross section of figure 9.

With Cohen’s distribution the plot is asymmetric with respect to $\epsilon(\theta_{med})$ and $\epsilon(\theta_{max})$: when $\epsilon(\theta_{min})$ is big, i.e., the fastest electron is scattered into the forward direction, then the energy of the electron with the biggest angle is higher than that of the electron with the intermediate θ_{med} . This region is marked with “1” in figure 10(a). And then there is a whole band of events near the right side of the triangle, labelled with “2”, where $\epsilon(\theta_{max})$ is very small and $\epsilon(\theta_{med})$ is the biggest. This corresponds to the central region of scattering angles in figure 7: the projectile, which is not the fastest electron any more, is emitted under small angles and one of the target electrons got a large transfer of energy from the projectile.

With the microcanonical distribution, figure 10(b), it can be seen again that events for small ϵ_i are missing. The plot is more symmetric, too. In region “1” both $\epsilon(\theta_{med})$ and $\epsilon(\theta_{max})$ are about equal, the correlation between the scattering angle and the final energy of the two slow electrons is nearly gone. Region “2” is similar to panel (a), though: this could already be expected from the angular distribution of the fastest and the projectile electron — which was not shown for the microcanonical distribution. This symmetry between the two slow electrons continues from high values of $\epsilon(\theta_{min})$ to low values: region “3”, which is essentially empty for Cohen’s distribution, is nearly as important as “2”: this, too, shows that the correlation between final angles and energies is much less pronounced for the “constructed” microcanonical distribution than for the more quantal distribution according to Cohen.

The corresponding plot from the product distribution again looks like a blurred version of the result from Cohen’s distribution: it is not shown here.

From figure 10(a) two modes can be inferred, in which the three electrons leave

the nucleus: in region “1” the fastest electron is emitted into the smallest angle, then comes the slowest electron and the electron with the intermediate energy leaves with the biggest angle; the slowest electron is between the faster ones. In region “2” this pattern is reversed: the fastest electron is between the two slower ones, but again with the bias that high final energies prefer small scattering angles.

The analogous pattern is observed when the relative angles between the electrons’ momenta in their center of mass system are plotted in a Dalitz plot. Then, one finds that the electron that is scattered into the most forward direction has preferentially the highest energy, followed by the one scattered into the most backward direction. The electron inbetween gets the smallest amount of energy. These plots are not shown here, because they provide no more information than the ones of figure 10.

Summarizing one can say that at this rather low impact energy of 250 eV, where the total energy of the whole system is just about twice as large as the target’s binding energy, the double ionization dynamics is much more complex than at high energies. There the projectile is very fast and can be reduced to a sudden perturbation, whereas it here is — classically speaking — only twice as fast as the target electrons. Now after the reaction the fastest electron is not necessarily the former projectile any more, as we have seen from the angle differential one electron cross section. This distinction is of course only possible in our classical treatment, but not in the experiment.

The doubly differential one electron cross section indicates two emission patterns: fast electrons essentially show up in a cone of about 20° around the forward direction, while the slow electrons are emitted into the rear half sphere. The crossover between these two regimes takes place at electron energies of 50 to 60 eV, at about a third of the total energy.

Due to the low yield of double ionization trajectories and the high dimensionality of the three–electron final state phase space we could not extract fully differential cross sections from these calculations, but correlation effects between the electrons’ final angles and energies can already be observed: high energies go with small angles, as already shown, and the scattering angle of the slowest electron is between the two faster ones — or the other way around: the fastest electron emerges between the two slow ones.

This cross sections again emphasizes that also at this low impact energy it is important to use an initial state distribution which reproduces the wave function as closely as possible, i.e., one which is derived from the quantum wave function. We see differences in the quality of the obtained cross sections between Cohen’s distribution and the product description, but the general results are the same, whereas the microcanonical distribution, which is constructed from a classical background, leads to artifacts and gives different results when it comes to the correlation between the electrons.

4. Summary

In this paper we demonstrated that our quasiclassical ansatz allows to calculate meaningful total and differential ionization cross sections on helium targets by means of a classical trajectory method. To this end we first explained how the algorithm [11], which initially had been developed with the hydrogen target, has to be adapted for many electron targets. It is especially important not to neglect the initial backward propagation that arises from translating the scattering operator from the quantum Møller formulation to its classical form. The resulting dynamical stabilization of the

autoionizing classical many electron target had been demonstrated already in a recent letter [12], together with the total cross sections for single *and* double ionization.

In this paper we took a closer look at the calculated total double ionization cross section and concluded from its $1/E^2$ high energy behavior that the dominant process for double ionization consists of two independent encounters between the projectile and the two target electrons (the “TS2” process). This conjecture was then confirmed by comparing our differential cross sections to experimental results at 2 keV impact energy. Both the relative angle between the two slow electrons and their joint energy distribution show no signatures of the sequential “TS1” process, but the cross sections are easily explained if only the “TS2” process takes place.

For impact energies below about 300 eV the total cross section $\sigma^{(2)}$ reproduces the experiment amazingly well. Therefore classical calculations should focus on this low energy regime, where it is hard to perform quantum calculations. Though there are no experiments available yet, we presented single and double differential cross sections at 250 eV.

In a classical calculation it is possible to label the electrons. With the calculations at 250 eV we showed that at low impact energies the identification of the fastest electron with the projectile starts to break down. Combining the three electrons’ relative energies into one plot we could identify a pattern, in which the electrons’ energies are “interleaved” with their scattering angle out of the forward direction: when the electrons are sorted according to their scattering angle then either the electron with the highest or with the lowest final energy is the middle one, but it is relatively unlikely that, e.g., the electrons’ energies decrease monotonically with increasing angle. Of course, we are anxious to see, whether the experiment will confirm our predictions — or not.

When performing the calculations on hydrogen it had been important to choose a phase space description for the target atom that best describes those features which are important in the corresponding energy range. We therefore ran the calculations on helium with three different initial distributions, too: two derived from the quantum wave function and one built from a classical approach. The two quantum derived distributions only differ in the quality of the resulting cross sections, whereas the classically derived one leads to artifacts, which clearly stem from its conceptual limitations. Consequently it is important to choose — within the constraints of feasibility and numerical effort — the best initial phase space distribution possible for the target: the classical calculation itself is a rather crude approximation, when it comes to the quantum contributions to the cross sections, but an inappropriate initial state will spoil even the classical parts.

The cross sections shown here are by no means exhaustive and at 250 eV they still have to be confirmed by experiment. They demonstrate that it now is possible to perform classical trajectory calculations on multi electron targets, in this case on helium, and that they yield reasonable results. These classical calculations will eventually not explain every single feature of any arbitrary cross section, but as they reproduce the classical parts of the reaction’s outcome they guide the identification of the quantum reaction paths and contributions to the complex low energy dynamics and cross sections.

It should be emphasized that this quasiclassical ansatz is very similar to standard CTMC and that it is easy to include the initial backward propagation to stabilize arbitrary unstable initial target descriptions into existing CTMC codes — only the interpretation of each single trajectory as one realization of the actual experiment has

to be discarded. Cross sections are, as in a discretized quantum approach, calculated only from the whole set of the trajectories' final values.

Further work will focus on the region of very low impact energies to see how the predicted power law at the threshold will be reproduced and how good the absolute cross sections coincide with experimental results.

This work was funded by the Israel Science Foundation. The author wants to thank Alexander Dorn for providing the experimental cross section of figure 5(a) in tabulated form.

References

- [1] R E Olson and J Fiol, *J. Phys. B: At. Mol. Opt. Phys.* **36** (2003) L365
- [2] R Abrines and I C Percival, *Proc. Phys. Soc.* **88** (1966) 861
- [3] C L Kirschbaum and L Wilets, *Phys. Rev. A* **21** (1980) 834
- [4] J S Cohen, *Phys. Rev. A* **54** (1996) 573
- [5] G Tanner, K Richter and J M Rost, *Rev. Mod. Phys.* **72** (2000) 497
- [6] J Zakrzewski, S Saini and H S Taylor, *Phys. Rev. A* **38** (1988) 3877
- [7] E B Bogomolny, *Nonlinearity* **5** (1992) 805
- [8] D Eichenauer, N Grün and W Scheid, *J. Phys. B: At. Mol. Phys.* **14** (1981) 3929
- [9] J S Cohen, *J. Phys. B: At. Mol. Phys.* **18** (1985) 1759
- [10] D J W Hardie and R E Olson, *J. Phys. B: At. Mol. Phys.* **16** (1983) 1983
- [11] T Geyer and J M Rost, *J. Phys. B: At. Mol. Opt. Phys.* **35** (2002) 1479
- [12] T Geyer and J M Rost, *J. Phys. B: At. Mol. Opt. Phys.* **36** (2003) L107
- [13] J E Moyal, *Proc. Cambridge Phil. Soc.* **45** (1949) 99
- [14] J S Cohen, *J. Math. Phys.* **7** (1966) 781
- [15] J R Taylor, *Scattering Theory*, John Wiley & Sons, Inc., 1972
- [16] E Wigner, *Phys. Rev.* **40** (1932) 749
- [17] J C Slater, *Proc. Natl. Acad. Sci.* **13** (1927) 423
- [18] E A Hylleraas, *Z. Phys.* **48** (1928) 469
- [19] E A Hylleraas, *Z. Phys.* **54** (1929) 347
- [20] C L Pekeris, *Phys. Rev.* **112** (1958) 1649
- [21] T Kinoshita, *Phys. Rev.* **115** (1959) 366
- [22] F Sattin, *arXiv:physics/0304055*
- [23] R L Becker and A D MacKellar, *J. Phys. B: At. Mol. Phys.* **17** (1984) 3923
- [24] M J Raković, D R Schultz, P C Stancil and R K Janev, *J. Phys. A: Math. Gen.* **34** (2001) 4753
- [25] M B Shah, D S Elliot, P McCallion and H B Gilbody, *J. Phys. B: At. Mol. Opt. Phys.* **21** (1988) 2751
- [26] Sir J J Thomson, *Phil. Mag. S. 6* **23** (1912) 449
- [27] M Inokuti, *Rev. Mod. Phys.* **43** (1971) 297
- [28] D R Schultz, L Meng and R E Olson, *J. Phys. B: At. Mol. Opt. Phys.* **25** (1992) 4601
- [29] J H McGuire, *Phys. Rev. Lett.* **49** (1982) 1153
- [30] A Dorn *etal*, *Phys. Rev. A* **65** (2002) 032709
- [31] R Rejoub, B G Lindsay and R F Stebbings, *Phys. Rev. A* **65** (2002) 042713
- [32] T Pattard and J M Rost, *Phys. Rev. Lett.* **80** (1998) 5081
- [33] P L Bartlett, A T Stelbovics and I Bray, *Phys. Rev. A* **68** (2003) 030701(R)
- [34] A Lahmam–Bennani, A Duguet and S Roussin *J. Phys. B: At. Mol. Opt. Phys.* **35** (2002) L59
- [35] A Dorn *etal*, *Phys. Rev. Lett.* **82** (1999) 2496
- [36] A Dorn, private communication
- [37] T Schneider, P L Chocian and J M Rost, *Phys. Rev. Lett.* **89** (2002) 073002
- [38] A Dorn *etal*, *Phys. Rev. A* **68** (2003) 012715
- [39] R H Dalitz, *Philos. Mag.* **44** (1953) 1068
- [40] L M Wiese, O Yenen, B Thaden and D H Jaecks, *Phys. Rev. Lett.* **79** (1997) 4982
- [41] M Schulz *etal*, *Phys. Rev. A* **61** (2000) 022703